High-Performance Dual Raman Spectrometer*

G. TEJEDA, J. M. FERNÁNDEZ-SÁNCHEZ, and S. MONTERO†
Instituto de Estructura de la Materia, CSIC, Serrano 123, 28006 Madrid, Spain

The transformation of an old Raman double monochromator into a dual spectrometer capable of working either as the original instrument or as a very high sensitivity scanning single monochromator with multichannel charge-coupled device (CCD) array detection is described. The merits and limitations of this instrument, particularly suited for medium/low resolution (0.3 to 2 cm^{-1}) Raman spectroscopy in the gas phase, are discussed. Example spectra of O_2, N_2, CO_2, H_2O, and CCl_4 are shown.

Index Headings: **Raman; Spectrometer; CCD; Gas.**

INTRODUCTION

Well-established merits of spontaneous Raman spectroscopy are the extensive spectral range accessible with standard instrumentation, the linear relation between intensities and density of scattering units at the sample, the usually sharp shape of bands due to totally symmetric normal modes, the small sampling size required, and the universality, in the sense that all molecular species contribute to Raman scattering.

Spontaneous Raman scattering is a two-photon process of intrinsically low efficiency in terms of the number of scattered photons per exciting photon irradiating the sample. With conventional instrumentation this condition means, in practice, a signal-to-noise ratio usually below 10^4. This limitation is particularly severe in samples with a low density of scattering units, such as gases, or highly diluted solutions. Therefore it is acknowledged that gas-phase linear Raman spectroscopy is a nonroutine technique. Most practical applications require a monochromator with a resolution of at least 1 cm^{-1}, with a continuous-wave (cw) laser source supplying a power of at least 2 W in a single line in the visible region. An efficient detection system is also mandatory, based on either a low-noise thermoelectrically cooled photomultiplier tube (PMT) operating in the photon-counting mode or, as a more recent option, on a charge-coupled device (CCD) bidimensional array detector working in the multichannel mode. The advantages of CCD detection, along with appropriate scanning methods for Raman spectroscopy, have been recently reported.[1]

In the present paper we describe the transformation of an old (1971) subtractive double monochromator into a dual instrument capable of working either as the original instrument (single channel) or, by modification of the internal optical path, as a single monochromator with scanning multichannel detection. The additional optics required for this modification are mounted on kinematic bases and can easily be installed or removed to switch from one configuration to the other. Single-channel and multichannel modes will henceforth be referred to as PMT and CCD modes, respectively.

In the PMT mode as a subtractive double monochromator, the instrument fully maintains its original capability for recording spectra from scatterers with a high level of stray light, such as polycrystalline or amorphous samples. In the CCD mode, the instrument is particularly suited for gas-phase spectroscopy, with an overall gain in sensitivity of about two orders of magnitude with respect to the original single-channel subtractive configuration. For gas samples consisting of diatomic, or small, polyatomic molecules, the detection limit of the instrument is attained at a pressure on the order of 0.1 Pa and is still better for larger molecules, especially if they include heavy atoms. Such a level of sensitivity makes the instrument particularly suited to record good-quality Raman spectra from rarefied media, such as the room-temperature gas phase of samples with low vapor pressure or the very low temperature and very low density gas phase characteristic of supersonic molecular jet environments.

SPECTROMETER

The original instrument was a Jarrell Ash 25-100 double Czerny–Turner scanning spectrometer with an f = 100 cm focal length and effective aperture ratio of f/8.7, with two identical diffraction gratings mounted on a common shaft. In a previous upgrading (1985), the original aluminum ruled gratings of 1180 grooves/mm had been replaced by holographic gratings of 2360 grooves/mm, doubling the resolving power.

Optical Path. In the original PMT mode (subtractive mounting), shown in Fig. 1a, the grating $\mathbf{G_1}$ is the dispersive one, while the grating $\mathbf{G_2}$ recombines those wavelengths passing through the intermediate slit $\mathbf{S_2}$. The monochromated radiation is detected by the photomultiplier (**PMT**) located behind the exit slit $\mathbf{S_3}$. Important advantages of this configuration are the high efficiency of stray light rejection and the low distortion of spectral band shapes recorded at narrow slits ($\leq$50 μm).

The subtractive mounting principle is not compatible with multichannel detection, which requires real images of the entrance slit $\mathbf{S_1}$, spatially resolved for different wavelengths, on the plane of the detector array. Therefore, for the multichannel configuration the optical path was adjusted by 90° by the mirror **M** in Fig. 1b, to reach the detector surface without being recombined by the second grating $\mathbf{G_2}$ of the monochromator. In both PMT and CCD modes, the dispersive element is the grating $\mathbf{G_1}$, which determines the limit of spectral resolution.

Detectors. The detector for the PMT mode is an RCA 31034A-02 selected photomultiplier tube. The dark current is reduced by thermoelectrical cooling to −25 °C. The signal is detected in photon-counting mode and, at

Received 23 April 1996; accepted 8 July 1996.
* Dedicated to the memory of Joseph Brandmüller (March 28, 1921–December 26, 1995), master and friend.
† Author to whom correspondence should be sent.

0003-7028/97/5102-0265$2.00/0

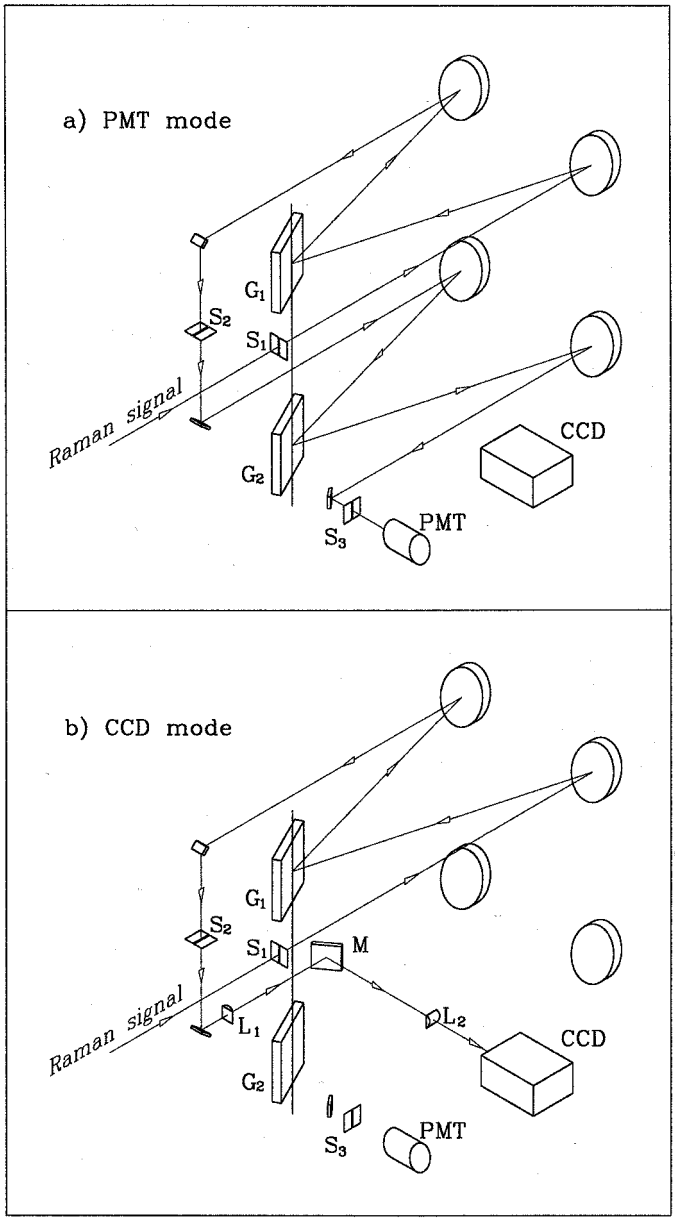

FIG. 1. Optical path of the dual spectrometer. **(a)** PMT mode with single-channel subtractive configuration; **(b)** CCD mode with multichannel configuration.

a working dc voltage of 1700 V, the residual background noise is usually kept below 5 count s^{-1}.

In the CCD mode an EGG 1530-C camera is used as a detector. It is equipped with a Thompson CSF THX-31159A front-illuminated four-phase CCD chip of 512 × 512 pixels, with a pixel size of 19 × 19 μm^2. The chip is refrigerated by liquid N_2, and at −110 °C the noise of the dark current is less than 0.0007 count s^{-1} $pixel^{-1}$. In addition, a readout noise of 1 count·$read^{-1}$ must be considered. A representative value of the quantum efficiency equivalence of this detector is 0.1 count/photon at 650 nm. This factor allows approximate conversion of the Raman intensities into the photonic flux, i.e., the number of photons arriving per second at a channel of the detector. A detection channel is defined by grouping adjacent pixels (binning) into rectangular units of $n_h \times n_v$ pixels, whose charge is summed up prior to the readout. The A/D converter of the detector has 18 bits, with a dynamical range of 262144 in a single readout, and a departure from linearity claimed to be smaller than 1% by the manufacturer. The nonuniformity of response across the detector is ±3%.

Scanning System. According to the manufacturer, the accuracy of the sinus-drive scanning system of the original instrument was not better than ±1.5 cm^{-1}, and its repetitivity for two consecutive scans not better than ±0.5 cm^{-1}. After years of wear, the previous figures had worsened considerably, and the accumulation of spectra to improve the signal-to-noise ratio was limited to a small number of scans at very low resolution. In an effort to overcome this limitation, a new scanning system has been devised on the basis of a high-accuracy micropositioning translational stage of 100 mm traveling distance and elementary step of 0.1 μm, actuated by a stepping motor. The linear displacement of the stage is transformed into the angular motion of the gratings shaft by means of a lever and a smooth-sliding mechanism. The motion is governed from a 486 PC via a GPIB interface by means of the scanning and data acquisition program REGISTRA, written in Turbo C (Borland), specifically developed for the present instrument. The present scanning mechanism is no longer a sinus drive (linear in wavelength) or a cosecant drive (linear in wavenumber). The position of the translational stage is converted into wavenumbers by REGISTRA, by means of an empirical fourth-order polynomial function. The current spectral range of the instrument is from 23,580 to 13,650 cm^{-1}; however, if required, this range can be globally shifted towards the blue or towards the red. This procedure, however, implies a complete redetermination of the calibration and wavenumber polynomial functions of the instrument.

The repetitivity of the system is better than ±0.03 cm^{-1} for two consecutive scans, and better than ±0.1 cm^{-1} for a large number of consecutive scans recorded in a period of up to six hours, regardless of the scanning conditions. An example of the actual repetitivity of multiple short consecutive scans, the most unfavorable scanning regime, is shown in Fig. 2, where $\Delta\nu$ is the observed shift of a reference sharp spectral line, and t the total time, including the fast rewind motion to the initial scanning position. Multiple scans can directly be accumulated if the resolution requirements are not too demanding (about 1 cm^{-1}). Otherwise, the observed drift must be corrected via software, by slightly shifting the wavenumbers of each spectrum with respect to a calibrated reference.

The program REGISTRA allows for a quick wavenumber calibration of the instrument by recording a reference line of known wavenumber. This step guarantees an accuracy of ±0.05 cm^{-1} for the next scan up to 200 cm^{-1} from the reference line, and ±0.15 cm^{-1} for a scan of up to 3000 cm^{-1}.

Multichannel Transfer Optics. For an optimal performance of the CCD multichannel detector, the size of the images of the entrance slit S_1, one for each wavelength passing throughout the intermediate slit S_2, must not exceed the horizontal and vertical dimensions of the detection channels of the chip, so that the width of the image covers at least three channels. This is done by means of the transfer optics consisting of the crossed cy-

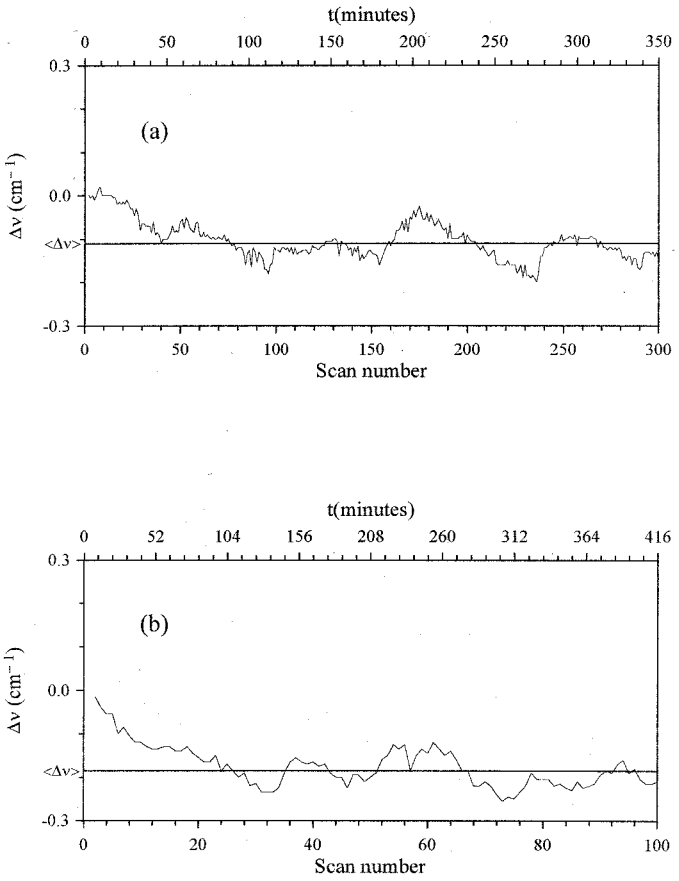

FIG. 2. Repetitivity of the scanning system in the CCD mode, referenced to a spectrum of 25 cm^{-1}: **(a)** 300 scans at a rate of 1 min/spectrum; **(b)** 100 scans at a rate of 4 min/spectrum.

lindrical lenses $\mathbf{L_1}$ and $\mathbf{L_2}$, and the flat mirror **M**, shown in Fig. 1b.

The dimensions of the entrance slit $\mathbf{S_1}$ are the adjustable width w_1 (10 μm $\leq w_1 \leq$ 3000 μm) and the adjustable height h_1 ($h_1 \leq$ 20 mm). The theoretical spectral resolution provided at $w_1 = 20$ μm by the dispersive element of the monochromator, the first grating ($\mathbf{G_1}$), is about 0.25 cm^{-1} near the exciting line at 514.5 nm and 0.16 cm^{-1} at 3000 cm^{-1} away in the Stokes side. In order to approach these figures as closely as possible, a transfer optics device of horizontal magnification $|\beta_h'| > 1$ is required. Otherwise, the image of the entrance slit $\mathbf{S_1}$ onto the phase of the detector would be about one pixel wide (19 μm) or even narrower, causing a severe loss of information about the spectral band shape, as well as a distortion of the observed profile. Two different methods have been proposed before to overcome this problem—one based on the numerical processing of the data,[2] and the other on the scanning procedure of the spectrometer.[1] The alternative solution to this problem, proposed here, is based on an optical design of the spectrometer using a magnification $|\beta_h'| = 2.3$ and is independent of any numerical algorithm.

On the other hand, at a slit height $h_1 = 20$ mm, a reduction of the vertical dimension of the image of $\mathbf{S_1}$ is required in order to not exceed the vertical dimension of the detector (9.7 mm). These two conditions are satisfied by means of the transfer optics shown in Fig. 1b. The

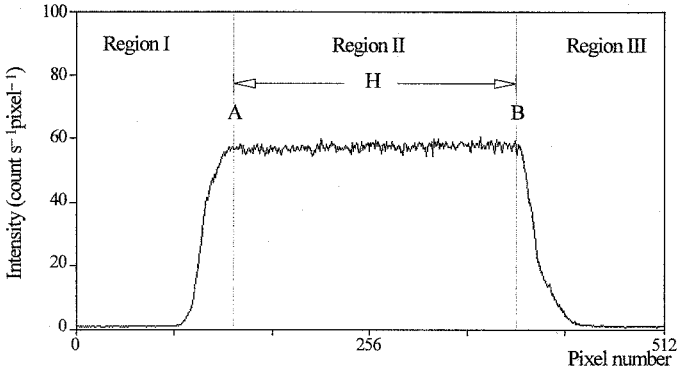

FIG. 3. Transfer function of the spectrometer in the CCD mode for $w_1 \ll w_2$ and $w_2 > 250$ μm; w_1 and w_2 are the widths of entrance slit, $\mathbf{S_1}$, and intermediate slit, $\mathbf{S_2}$, respectively.

crossed cylindrical lenses $\mathbf{L_1}$ and $\mathbf{L_2}$ produce horizontal and vertical magnifications of $\beta_h' = -2.3$ and $\beta_v' = -0.45$, respectively. In this way, any Raman photon passing through the intermediate slit $\mathbf{S_2}$ arrives at the CCD detector.

The intermediate slit $\mathbf{S_2}$ acts to some extent as a stray light filter. Its variable width w_2 allows selection of a narrow spectral interval, which is projected onto the active surface of the detector by means of the transfer optics. The instrumental transfer function is defined as the transmitted intensity vs. the wavenumber, or its equivalent pixel position. For a particular setting of the slits $\mathbf{S_1}$ and $\mathbf{S_2}$, at widths w_1 and w_2, this function is obtained by illuminating the entrance slit $\mathbf{S_1}$ with a source of white light. For $w_1 \ll w_2$, and $w_2 \geq 250$ μm, the transfer function has the trapezium-like shape shown in Fig. 3. For the present purpose, only the region A–B of flat transmittance is used. On the basis of geometry, horizontal magnification β_h', pixel size, and shape of the slit function, its width, expressed in number of pixels, is

$$H = \beta_h'(250 - w_2)/19 \qquad (1)$$

with w_2 expressed in μm. Signals from regions I and III are ignored in the scanning and detection processes, described in the next section. For the maximum width of $\mathbf{S_2}$, $w_{2max} = 3000$ μm, and for the horizontal magnification $\beta_h' = -2.3$, the useful width of the image is $H = 332$ pixels, covering about 65% of the horizontal dimension of the detector. Larger coverages can in principle be attained for $|\beta_h'| > 2.3$ but at the cost of increasing the curvature aberration in the image plane. The choice $\beta_h' = -2.3$ represents a compromise between detection efficiency and quality of image. The latter is of crucial importance for the wavenumber accuracy in the CCD mode.

The spectral bandpass interval corresponding to H according to Eq. 1 will henceforth be designated as spectral window $\delta(\nu)$. It depends on the wavenumber ν of the radiation passing through the center of the intermediate slit $\mathbf{S_2}$. For $w_2 \geq 250$ μm, this dependence is given by

$$\delta(\nu) = 10^{-4}(w_2 - 250)(\nu/f)\sqrt{\nu^2 d^2 - 0.25} \qquad (2)$$

where $f = 100$ cm is the focal length of the spectrometer, and $d = 4.23728 \times 10^{-5}$ cm, the groove spacing of the grating $\mathbf{G_1}$. For ν in cm^{-1} and w_2 in μm, the spectral window $\delta(\nu)$ is expressed in cm^{-1}. In practice, a slit width $w_2 = 2600$ μm is used for most applications. The spectral

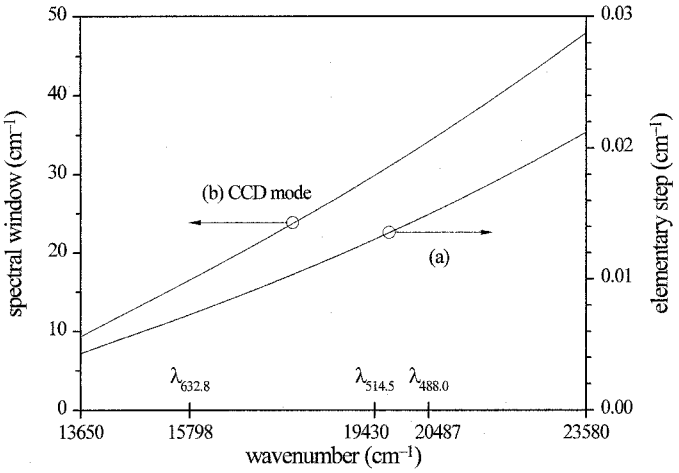

FIG. 4. (***a***) Wavenumber equivalence of the elementary step (0.1 μm) of the scanning system, and (***b***) wavenumber equivalence of the spectral window $\delta(\nu)$ in the CCD mode at width $w_2 = 2600$ μm of the intermediate slit $\mathbf{S_2}$.

window $\delta(\nu)$ for $w_2 = 2600$ μm is shown in graph ***b*** of Fig. 4 for the useful range of the instrument.

Owing to the geometrical configuration and dimensions of the housing of the original instrument, we have been constrained to use lenses instead of mirrors for the transfer optics between the intermediate slit $\mathbf{S_2}$ and the CCD detector. Therefore, the horizontal and vertical magnifications β_h' and β_v' are slightly dependent on the wavenumber. The dependence of β_v' has no noticeable effects on the scanning and data acquisition. On the contrary,

$$\beta_h' = -2.63272 + 1.72583\nu \times 10^{-5}, \qquad (3)$$

with the wavenumber ν expressed in cm^{-1}, is important for the scanning control and wavenumber accuracy of the instrument. Through Eqs. 1, 2, and 3, β_h' has some influence on the scanning step size in the CCD mode, as described in the next section. Also the location of the image plane of the cylindrical lens $\mathbf{L_1}$ depends slightly on β_h' and, indirectly, on the wavenumber ν. In order to compensate for this effect when scanning large spectral intervals, the lens $\mathbf{L_1}$ is mounted onto a micropositioning translational platform actuated by remote control. This way, the image plane of $\mathbf{L_1}$ can be accurately refocused onto the active surface of the CCD detector if required. At a spectral resolution of 0.5 cm^{-1}, or better, this refocusing is necessary only for spectral intervals larger than 300 cm^{-1}. At lower resolution, or for spectral intervals smaller than 300 cm^{-1}, the effect is negligible. The effect of such refocusing on the wavenumber accuracy is negligible in practice, since it is automatically taken into account by the scanning and data acquisition program REGISTRA.

Scanning Modes and Data Acquisition. Depending on whether the instrument is operated in PMT mode or in CCD mode, the program REGISTRA provides different scanning options. Since the implementation of the multichannel detection is the main innovation of present paper, we describe next in some detail the procedure to record spectra in the CCD mode. The procedure in the PMT mode is the usual one for a scanning system driven by a stepping motor. However, in both modes the scanning is defined by the following main parameters:

- *WI* and *WF*: Absolute wavenumbers of the initial and final points of the spectrum, with $WI < 23{,}580$ cm^{-1}, $WF > 13{,}650$ cm^{-1}, and $WI > WF$.
- *N*: Number of scans of the $WI \rightarrow WF$ spectrum, with $1 \leq N \leq 1296$.
- *STEP*: Scanning step size (see below).
- *DAP*: Data acquisition period between steps, expressed in seconds, with $0.01 \leq DAP < 1000$.

The wide range of these parameters allows for great versatility in the working conditions. For better reproducibility of the spectra, data are acquired along each *DAP* while the scanning system is at rest between consecutive steps.

In the PMT mode, *STEP* is declared in units of the elementary step (0.1 μm) of the micropositioning translational stage of the scanning system, within the limits $1 \leq STEP \leq 999$. The equivalence of one elementary step in cm^{-1} is shown in graph ***a*** of Fig. 4. In the CCD mode, *STEP* is automatically identified with the spectral window defined by Eq. 2 [$STEP = \delta(\nu)$] by the program REGISTRA, which calculates the equivalent rotation angle of the grating's shaft for each STEP and transfers this information to the scanning system. According to Eq. 2, the spectral window $\delta(\nu)$ is defined by the intermediate slit width setting w_2. For routine scanning conditions, a recommended choice is $w_2 = 2600$ μm, which determines a window of about 284 pixels at the CCD detector, equivalent to the spectral window shown in Fig. 4b. The complete $WI \rightarrow WF$ spectrum is thus recorded in the CCD mode as an automatic concatenation of partial spectra, or "snapshots", each one covering a spectral window $\delta(\nu)$, with no loss or repetition of spectral data points.

An important advantage of scanning by spectral windows $\delta(\nu)$ on the order of 25 cm^{-1}, and *DAP* of typically 10–60 s, is the fact that any random fluctuation contributing to the signal or to the background—such as those from the laser power or from dust particles crossing the laser beam waist—is evenly distributed along the whole spectral window and averaged over the *DAP*. In this sense, the *DAP* acts as a kind of time constant without degrading the spectral resolution.

A two-column ASCII file is created by REGISTRA for each one of the *N* complete $WI \rightarrow WF$ spectra. The first column stores the wavenumbers, and the second column, the readout along the *DAP* for the channel of the CCD detector corresponding to each wavenumber. The consecutive spectra, up to $N = 1296$, are stored in independent files in order to minimize any loss of information caused by external disturbances. The discretization of wavenumbers (i.e., the number of rows in each file) is imposed by the magnification β_h' of the transfer optics according to Eq. 3 and by the pixel size of the detector (19 μm) or its multiples if the detector is binned (see below) in the horizontal direction. In terms of wavenumbers, the discrete intervals are approximately $0.1 \times n_h$ cm^{-1} near the exciting line at 514.5 nm and $0.07 \times n_h$ cm^{-1} at 3000 cm^{-1} away in the Stokes side, with n_h, the horizontal binning. For a Raman spectrum of 3000 cm^{-1} length, excited with the 514.5-nm line, this discretization at the lowest horizontal binning, $n_h = 1$, adds an uncertainty of ± 0.05 cm^{-1} to the other sources of uncertainty of the scanning system. On the whole, a conservative figure of

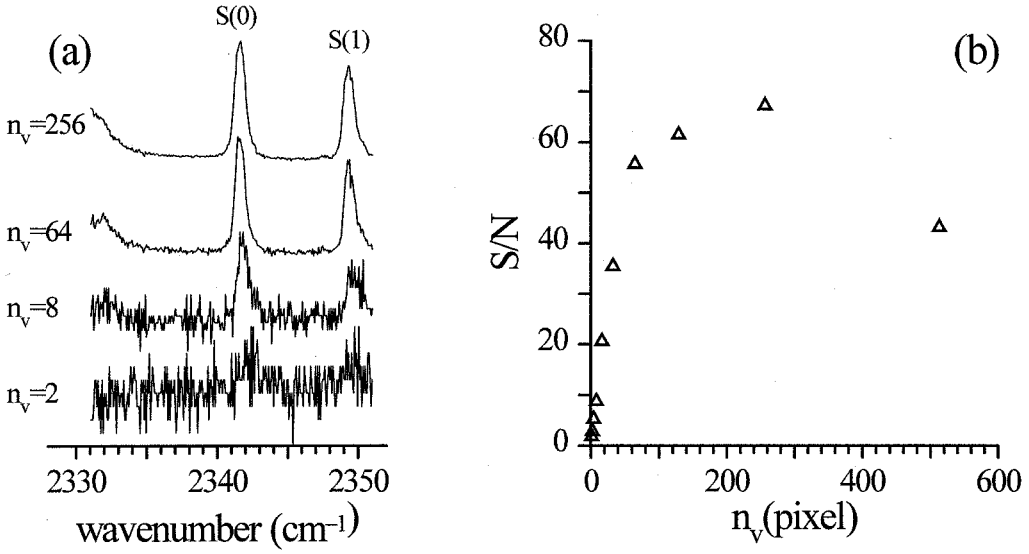

FIG. 5. **(a)** Effect of the vertical binning, n_v, on the S(0) and S(1) lines of the $v = 0 \rightarrow 1$ vibrational-rotational Raman band of $^{14}N_2$; **(b)** improvement of the signal-to-noise ratio (S/N) as a function of the vertical binning n_v.

± 0.1 cm^{-1} can be proposed for the wavenumber measurement accuracy of the instrument.

Binning in the CCD Mode. A peculiarity of CCD array detectors is the binning option, or grouping in tiles of $n_h \times n_v$ pixels, whose charge is added up prior to the readout process. In practical terms, each channel of the multichannel detector is defined by the product $n_h \times n_v$. As explained above, at liquid N_2 temperature the dark current of individual pixels is very low, and the main source of noise is the readout process. Therefore, the binning process, by reducing the number of readout operations, significantly improves the signal-to-noise ratio of the recorded spectra. In Fig. 5a an example of the efficiency of vertical binning is shown. The noticeable loss of linearity for $n_v > 100$ in Fig. 5b is due to the size and distribution of brightness of the image of the entrance slit $\mathbf{S_1}$ onto the image plane (the active surface of the CCD chip). Since this image on the CCD detector plane is due to the vertical entrance slit $\mathbf{S_1}$ of the monochromator, the binning of pixels in the vertical direction should in principle span the whole vertical dimension of the detector, i.e., $n_v = 512$ pixels. However, the vertical magnification of the transfer optics is $\beta_v' = -0.43$, and at full height of the entrance slit, $h_1 = 20$ mm, no more than approximately the 400 central pixels are illuminated. In addition, the illumination of the entrance slit is not homogeneous, because of the 90° excitation-collection geometry of the Raman experiment and the hyperboloid-like shape of the scattering region at the laser beam waist. Consequently, the density of Raman photons arriving at the equatorial line of the CCD array is larger than that at the upper or lower borders of the image. Hence, it is advantageous to constrain the vertical binning to a column of $n_v \leq 250$ central pixels, since the remaining pixels above and below this column are either not illuminated at all or are illuminated with a small density of Raman photons. As shown in Fig. 5b, we found empirically that a vertical binning of $n_v \leq 250$ central pixels—this number depending on the spectral resolution—optimizes the signal-to-noise ratio of the detection.

On the other hand, the spectrometer is not an optical centered system. The image of the straight vertical entrance slit $\mathbf{S_1}$ onto the detector surface is slightly curved. At full height $h_1 = 20$ mm of the entrance slit $\mathbf{S_1}$, the curvature of the image is noticeable for slit widths $w_1 < 100$ μm, and a vertical binning of 250 pixels implies a loss of resolution and a distortion of the spectral line shapes. This undesired effect can be minimized by reducing the entrance slit height to $h_1 = 5$ mm and the vertical binning to $n_v \leq 100$ central pixels. The global flux reduction of Raman photons arriving at the active portion of the detector can be compensated for by increasing the *DAP* by a factor $F = 250/n_v$. An effective resolution of ~ 0.3 cm^{-1} can be attained under these conditions, still with a very good sensitivity.

For slit widths $w_1 \geq 100$ μm, a horizontal binning $n_h \geq 2$ is recommended in addition to the vertical binning, in order to further improve the signal-to-noise ratio by almost a factor of n_h. A binning of $n_h = 6$ is still compatible with a spectral resolution of 2 cm^{-1}.

SAMPLE CHAMBER

The multichannel configuration of the spectrometer has been conceived with the aim of extending Raman spectroscopy into the realm of highly diluted gas-phase samples. Representative examples of these are the room-temperature spectra from samples with low vapor pressure and the spectra from gases under supersonic expansion regime, at very low temperature and density.

A serious limiting factor in Raman spectroscopy of diluted gases is the stray radiation from the optical windows and from the walls of the cell containing the gas sample. This effect is particularly severe if a multipass system[3] is used to increase the irradiance of the exciting laser beam onto the sample. In an effort to minimize the stray radiation, and also to allow for the recording of spectra from gases under a supersonic expansion regime, a large sample chamber of $42 \times 42 \times 24$ cm^3 has been

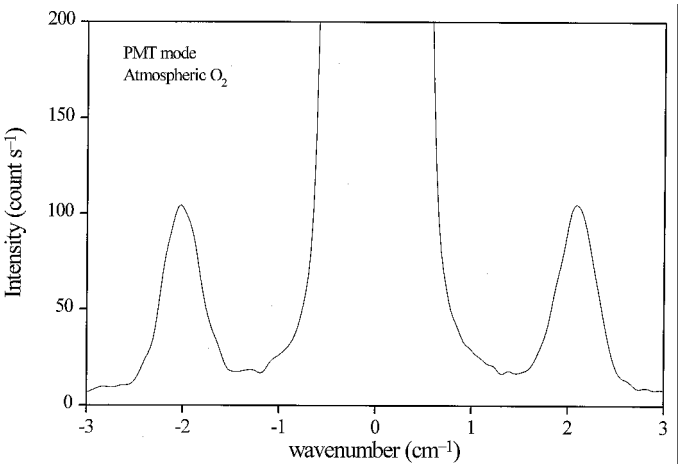

FIG. 6. Raman spectrum of the spin satellites of oxygen in ambient air *within* the sample chamber, recorded in the PMT mode. Scattering geometry: $X(ZX)Z + X(ZY)Z$; laser power 1 W at 514.5 nm, single pass; slits: $w_1 = w_2 = w_3 = 40$ μm; $h_1 = 20$ mm; *DAP* = 4 s; *STEP* = 2.

devised and commissioned.‡ The 90° exciting–collection optics is installed within this chamber. For the excitation it includes a multipass system, along with six micropositioning devices required for an efficient focusing of laser beam and multipass system. A photograpic objective with an $f = 50$ mm focal length and aperture of $f/0.95$, approximately equivalent to 1 srad, collects the Raman scattering, which is focused onto the spectrometer entrance slit $\mathbf{S_I}$ by an auxiliary lens with a focal length of $f = 500$ mm, external to the sample chamber. For better tightness, the micropositioning devices are actuated by remote control from outside the chamber. The working range of pressure inside the chamber is between 0.1 Pa and 200 kPa.

The chamber is connected to a gas-feeding line through a movable nozzle, and to a high-capacity vacuum line. The two optical windows of the chamber, one for the laser beam and the other for the Raman photons, are located, respectively, 16 and 26 cm away from the sharp focal region where the Raman photons are scattered by the gas sample. No spurious Raman spectrum from glass windows is observed, even under the most demanding conditions. The global level of stray light in the chamber is very low, and spectra like that in Fig. 6, showing—neatly resolved—the two spin satellite lines of molecular oxygen at ±2 cm^{-1} from the exciting wavenumber, can be recorded in the PMT mode. In the CCD mode, where the stray light rejection of the spectrometer is poorer, good-quality pure rotational Raman spectra can be recorded 5 cm^{-1} away from the exciting wavenumber, as shown in Fig. 7b. For spectral regions more than 200 cm^{-1} away from the exciting wavenumber, the use of a notch filter proves useful, as it further reduces the influence of the monochromatic stray light from the chamber. The signal-to-noise ratio improves by a factor of about 1.5 with the aid of the notch filter.

Gas-phase spectra from liquids of low vapor pressure can be recorded in many cases at room temperature, by placing a small vessel with the liquid sample within the chamber, evacuating the chamber for a few minutes, and allowing the vapor to reach the equilibrium pressure at the temperature of the laboratory. Good-quality spectra can be recorded at pressures as low as 100 Pa, and strong and sharp bands of most species can still be detected at 0.1 Pa. Spectra of gases under supersonic expansion are recorded by locating the expansion nozzle close to the focal point of the exciting laser beam. At a stagnation pressure of 100 kPa, strong and sharp lines in the spectrum can be neatly observed at a distance of 10 mm downstream from the nozzle,[4] where the molecular density number is on the order of 10^{21} molecule/m^3.

‡ A complete description of this sample chamber will be published.

EXAMPLES OF GAS-PHASE RAMAN SPECTRA

All spectra reported next were recorded *within* the sample chamber and are thus representative of the actual performance of the equipment.

The performance of the instrument in the PMT and CCD modes in the spectral region near the exciting line can be compared in the spectra from ambient air shown in Fig. 7. The spectra are shown as recorded, with no analogical or digital smoothing of the data. Both spectra were recorded with the same laser power (1 W), and entrance slit width ($w_1 = 50$ μm) and slit height ($h_1 = 20$ mm). With the exception of the region below 5 cm^{-1} from the exciting line, where the background of the spectrum recorded in the CCD mode is higher, both spectra are of comparable quality. The main difference between the two spectra is the measurement time, about 75 times shorter in the CCD mode than in the PMT mode. In the CCD mode, the borders between spectral windows of ~26 cm^{-1} (*DAP* = 10 s per spectral window) are marked by dotted lines.

In order to compare the spectral resolution in PMT and CCD modes, a detail is shown in Fig. 8 of the doublet at ~60 cm^{-1} recorded under appropriate conditions for better resolution. The $J = 6 \rightarrow 8$ transition of $^{14}N_2$ at 59.67 cm^{-1} and the $N = 9 \rightarrow 11$ transition of $^{16}O_2$ at 60.34 cm^{-1} are neatly resolved, both in PMT and in CCD modes. The effective full width at half-maximum (FWHM) attained, 0.28 cm^{-1}, is just slightly poorer than the theoretical value of 0.25 cm^{-1} of the instrument. It should be noticed that in the CCD mode this resolution can be achieved only by limiting the readout of the CCD detector in the vertical direction to the 25 central pixels, binned to $n_v = 25$. Even with this constraint, the spectrum recorded in the CCD mode required just 80 s, while the spectrum in the PMT mode required 600 s. Besides the gain in time, the signal-to-noise ratio is far better in the CCD mode.

An undesired side effect of the multichannel CCD detection arises from the cosmic radiation onto the detector. It generates an anomalously large charge at just a few pixels, giving rise to spikes, which appear randomly superimposed on the spectrum. For a CCD active area of 23 mm^2, the usual one under routine CCD scanning conditions, the average rate is on the order of one spike per minute per spectral window. Such peaks can be identified easily, as they are usually narrower than the true spectral lines observed at an instrumental half-bandwidth of 0.3 cm^{-1} or broader.

Several procedures for automatic remotion of spikes have been described in the literature.[5–8] However, in the

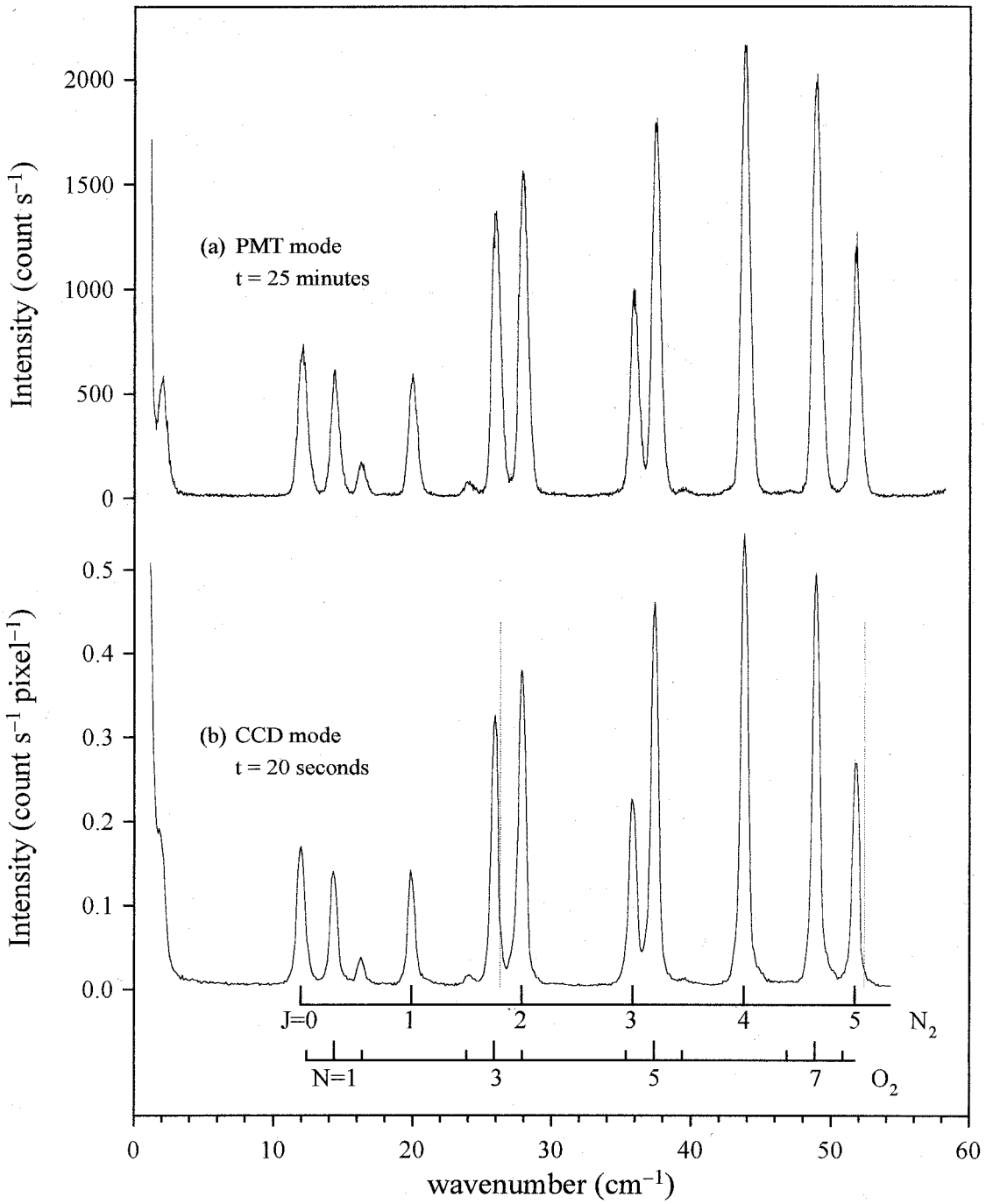

FIG. 7. Rotational Raman spectra of N_2 and O_2 in ambient air recorded *within* the sample chamber. Laser power: 1 W at 514.5 nm, single pass; (***a***) slits: $w_1 = w_2 = w_3 = 50$ μm; $h_1 = 20$ mm; (***b***) slits: $w_1 = 50$ μm, $h_1 = 20$ mm, $w_2 = 2600$ μm; binning: $n_h = 1$ pixel, $n_v = 50$ pixels. Dashed vertical lines indicate the borders between spectral windows.

present stage where the performance of the instrument is being tested, we have preferred to deal with this problem by recording the spectrum several times, at a *DAP* not longer than one minute, then identifying the spikes by visual inspection of the various scans, and eliminating the spikes by means of the spectra handling program MANEJO. Finally, the spike-free spectra are added to improve the signal-to-noise ratio. Two examples of this procedure are represented in Figs. 9 and 10, showing that spike elimination and spectra accumulation are fully compatible with a spectral resolution of about 0.3 cm^{-1}. In Fig. 9 the $v = 0 \rightarrow 1$ Q-branch of $^{16}O_2$ is shown, recorded as the accumulation of 10 spectra of *DAP* = 60 s each. The weak O(3) line at ~ 1542 cm^{-1} can be clearly identified, and no evidence of the eliminated spikes can be observed in the resulting spectrum. In Fig. 10 the $v = 0 \rightarrow 1$ Q-branch of $^{14}N_2$ is shown, recorded in the CCD mode as the result of accumulating 20 spike free spectra of *DAP* = 60 s each. Again, no evidence remains of the spikes present in the raw spectra.

One of the main difficulties related to the scanning procedure in the CCD mode is the accurate concatenation

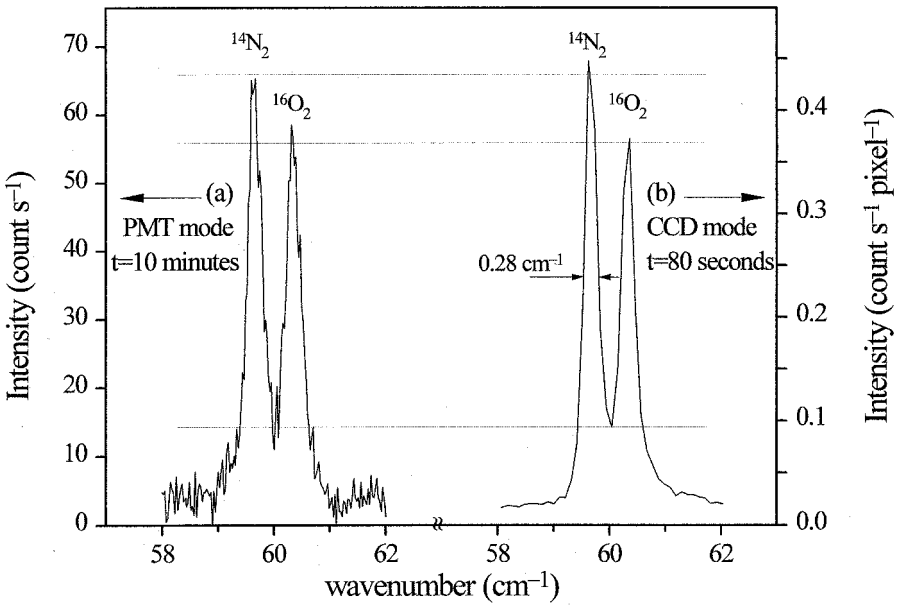

FIG. 8. Rotational Raman spectra of N_2 and O_2 in ambient air (detail). Laser power: 1 W at 514.5 nm, single pass. (***a***) slits: $w_1 = w_2 = w_3 = 18$ μm, $h_1 = 10$ mm; (***b***) slits: $w_1 = 20$ μm, $h_1 = 5$ mm, $w_2 = 2600$ μm; binning: $n_h = 1$ pixel, $n_v = 25$ pixels.

of the spectral windows corresponding to each *DAP*. A test of the automatic concatenation is shown in Fig. 11, where the complete $v = 0 \rightarrow 1$ vibrational rotational band of $^{16}O_2$ from an ambient air sample is displayed. The result shown is a single spectrum, recorded as the concatenation of 20 spectral windows of ~ 20 cm^{-1}. No distortion of the spectrum due to the scanning procedure can be detected.

Figures 11 and 12 provide a good example of the sensitivity of the spectrometer in the CCD mode. In Fig. 11 the upper component of the main Fermi diad of atmospheric $^{12}CO_2$ in the laboratory air can be identified at 1388.2 cm^{-1}. In Fig. 12 a detail is shown of the spectrum of atmospheric CO_2 in natural abundance. The ν_l and ν_u components of the main Fermi diad are observed with a good signal-to-noise ratio, and also its hot bands ν_l^* and ν_u^*, and the O(25), O(27), O(29), and O(31) lines of $^{16}O_2$ can be identified. The weak feature at 1369.9 cm^{-1} is the ν_u line of $^{13}CO_2$ isotopic species in the sample, 100 kPa of ambient air, with abundance of about 4 ppm. It is worth mentioning that the photonic flux from this line is less than 1 photon per second per channel. Since the number of spectra that can be accumulated is, in principle, a matter of time, and the laser power can still be increased to 7 or 8 W with a more powerful laser, it seems realistic to propose a figure of merit for the sen-

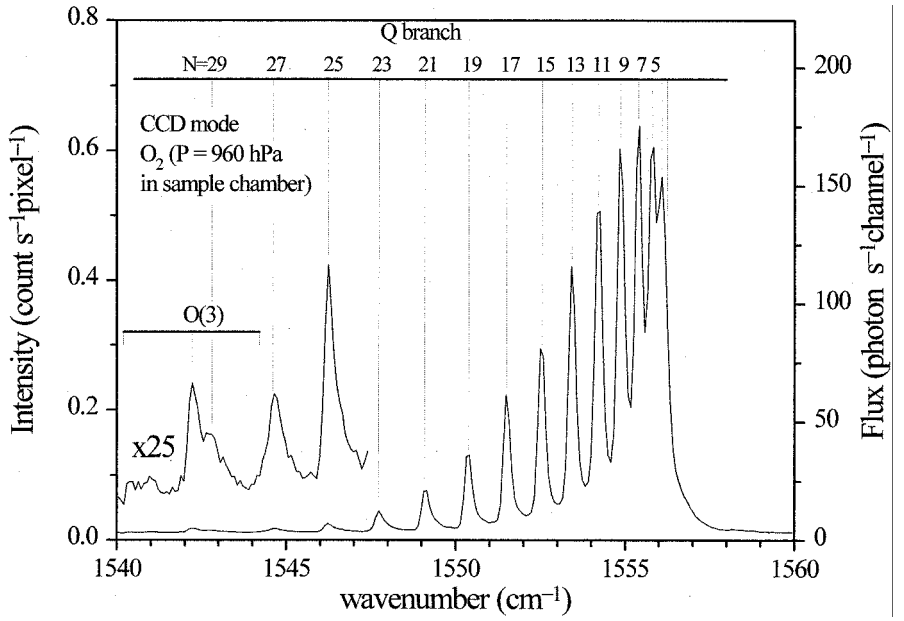

FIG. 9. Raman spectrum of the Q-branch ($v = 0 \rightarrow 1$) of $^{16}O_2$ recorded in the CCD mode. Sample pressure: $P = 960$ hPa. Laser power of 1.2 W (+ multipass + notch filter), at 514.5 nm. Average of $N = 10$ spectra at a rate of 1 min/spectrum; slits: $w_1 = 16$ μm, $h_1 = 5$ mm, $w_2 = 2600$ μm; binning: $n_v = 25$ pixels, $n_h = 1$ pixel.

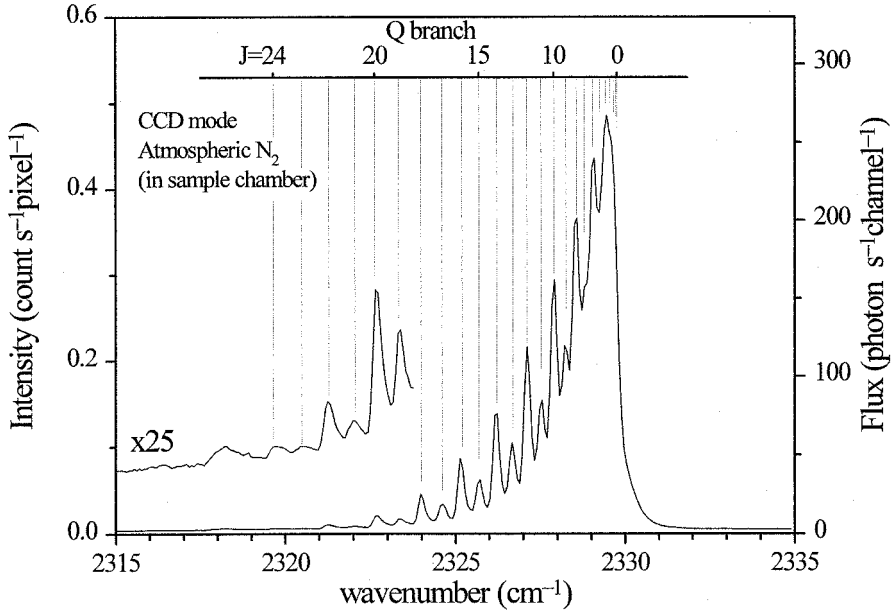

FIG. 10. Raman spectrum of the Q-branch ($v = 0 \rightarrow 1$) of N_2 in ambient air, recorded in the CCD mode. Laser power 1.5 W (+ multipass + notch filter); average of 20 spectra at a rate of 1 min/spectrum; slits: $w_1 = 20$ μm, $h_1 = 5$ mm, $w_2 = 2600$ μm; binning: $n_h = 1$ pixel, $n_v = 50$ pixels.

sitivity of the instrument on the order of 2.5×10^{19} molecules/m^3, for most molecular species in the gas phase.

An overview spectrum of the main Fermi resonance region of CO_2 recorded under routine conditions is shown in Fig. 13. The spectrum, recorded in a total time of 6.5 min, consists of 13 concatenated spectral windows $\delta(\nu)$ of ~21 cm^{-1} each, at $DAP = 30$ s. Because of the relatively high number of lines per spectral window, some lines lie in between two consecutive spectral windows. The borderlines between them are marked in Fig. 13 with dotted lines. No artifacts associated with the automatic concatenation can be observed in the spectrum. All lines appear equally smooth, which proves the accuracy of the scanning system and the efficiency of the algorithm converting the wavenumbers calculated for the borders of the spectral windows into the motion of the grating's shaft. This spectrum also provides a good test for the wavenumber accuracy of the instrument under routine conditions. With the use of the O(24) line at 1351.508 cm^{-1} as a reference,[9] the standard error of estimate for an ensemble of 77 well-defined single lines in the interval 1200–1500 cm^{-1} (overlapping lines, Q-branches, and lines that are too weak are excluded) with respect to the wavenumbers reported[9] is $S_y = 0.06$ cm^{-1}.

A detail of the region between 1256 and 1280 cm^{-1}, recorded at 200 hPa to minimize the pressure line broad-

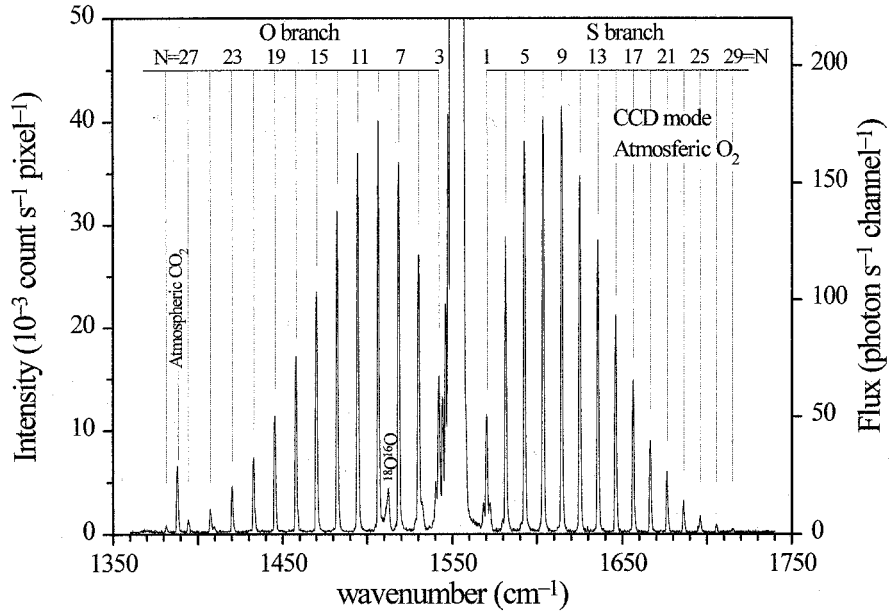

FIG. 11. Vibrational-rotation Raman spectrum of O_2 in ambient air, recorded in the CCD mode (one single spectrum in $t = 14$ min). Laser power 1.5 W at 514.5 nm (+ multipass + notch filter); slits: $w_1 = 100$ μm, $h_1 = 20$ mm, $w_2 = 2600$ μm; binning: $n_h = 2$ pixels, $n_v = 200$ pixels.

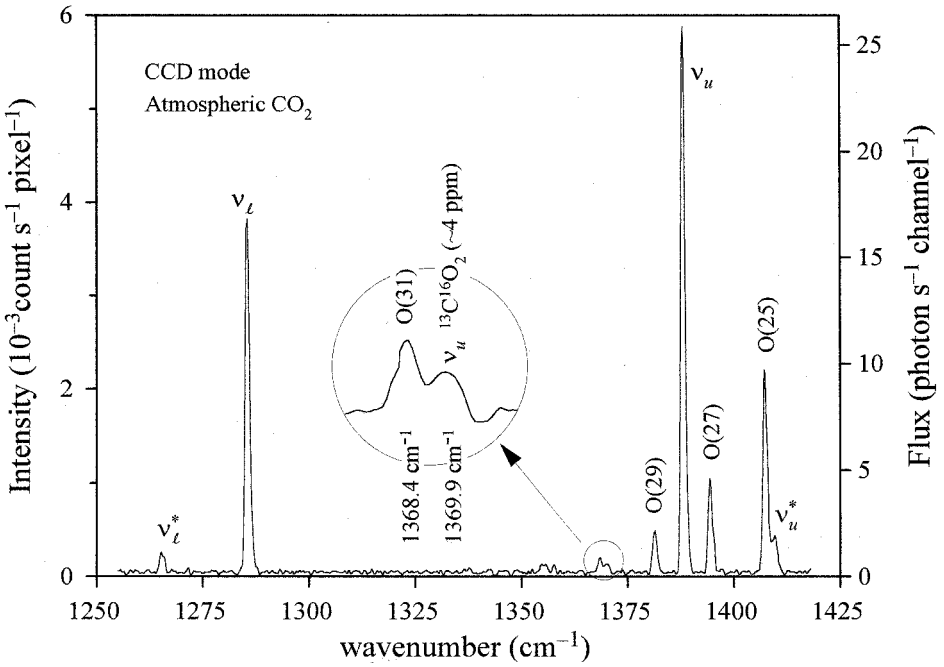

FIG. 12. Raman spectrum of CO_2 in ambient air, showing the O(25), O(27), O(29), and O(31) vibrational-rotational transitions of $^{16}O_2$, and the ν_u band of $^{13}C^{16}O_2$; ν_u^* and ν_l^* are the hot bands of the ν_u and ν_l Fermi diad. Same recording conditions as in Fig. 11, but averaging $N = 18$ spectra at a rate of 6 min/spectrum.

ening, is shown in Fig. 14. This spectrum is the average of 16 spectra, with a total recording time of 16 min. The ν_l Fermi components of the isotopic species $^{18}O^{12}C^{16}O$ and $^{17}O^{12}C^{16}O$ are observed at 1259.4 and 1272.3 cm^{-1}, respectively.[10,11] The low background noise of the accumulated spectrum allows observation of the $^{17}O^{12}C^{16}O$ species with a signal-to-noise ratio on the order of 10. The natural abundance of this species is 0.079%, which at 200 hPa corresponds to a molecular density number $\mathcal{N} = 4 \times 10^{21}$ molecules/m^3. This figure is a fraction of 1/5000 of the molecular density number at 100 kPa and 300 K—a measure of the possibilities of the instrument for the detection of molecular species at low concentration in mixtures with a highly dominant species of similar spectral pattern.

Because of the low molecular density number, gas-phase Raman spectra from low-vapor-pressure species are always a challenge for the experimentalist, and for many important molecular species no good-quality spectra have ever been reported. The molecular density number can be augmented, and hence the observed intensity as well, by increasing the temperature of the liquid sample and of the sample cell environment. Unavoidably, this approach leads to a broadening of the spectral lines and a noticeable loss of resolution. In Fig. 15 the Raman spectrum of the Q-branch of the ν_1 band of H_2O is shown. The spectrum, recorded at the vapor pressure of the laboratory ambient temperature, $P = 28$ hPa and 296 K, shows many features that remain unresolved in the spectrum reported in the literature,[12] recorded at a temperature of 400 K.

Gas-phase Raman spectroscopy at temperatures well

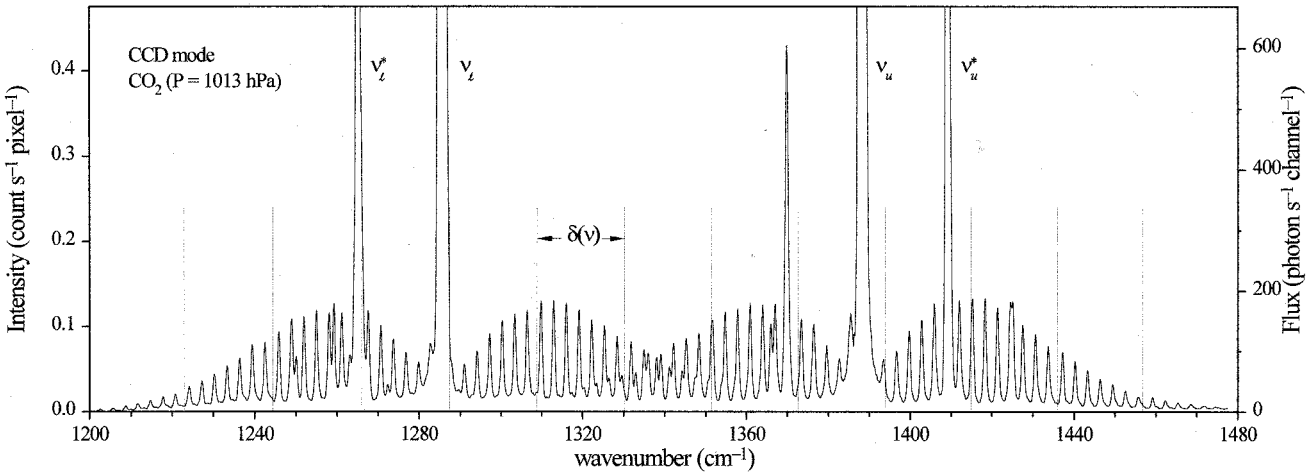

FIG. 13. Raman spectrum of CO_2 at $P = 1013$ hPa, recorded in the CCD mode under routine conditions (one single spectrum in $t = 390$ s); laser power 1 W at 514.5 nm, single pass; slits: $w_1 = 50$ μm, $h_1 = 20$ mm, $w_2 = 2600$ μm; binning: $n_h = 1$ pixel, $n_v = 128$ pixels.

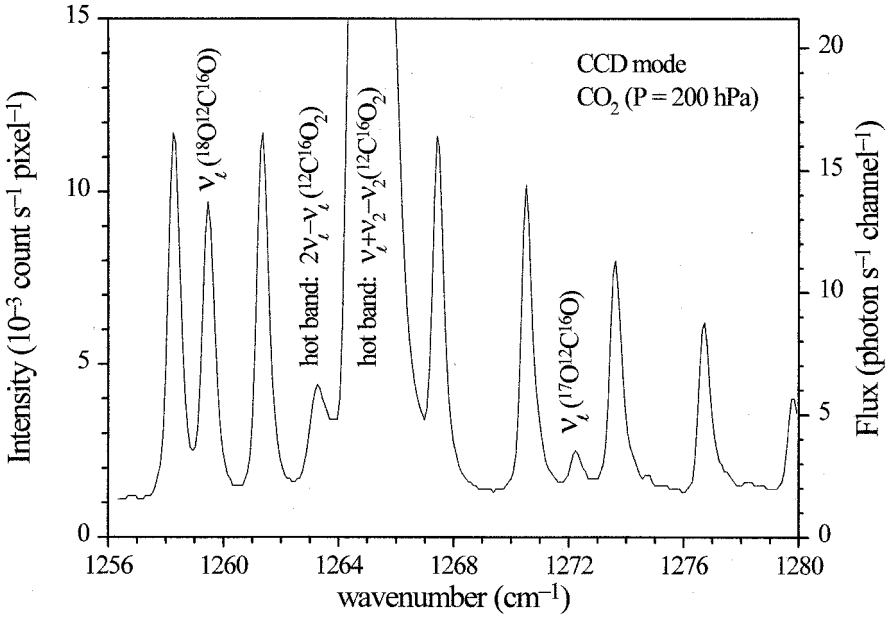

FIG. 14. Raman spectrum of CO_2 at P = 200 hPa recorded in the CCD mode. Detail showing the ν_1 component of the isotopic species $^{18}O^{12}C^{16}O$ and $^{17}O^{12}C^{16}O$; laser power 2 W at 514.5 nm (+ multipass); slits: w_1 = 30 μm, h_1 = 10 mm, w_2 = 2600 μm; binning: n_h = 1 pixel, n_v = 128 pixels; average of N = 16 spectra at a rate of 1 min/spectrum.

below the condensation point is possible under a supersonic expansion regime. However, under these conditions the molecular density number is very low, and only a few experiments of this kind have been reported.[14,15] Here we show how such spectra can be routinely recorded with the present instrument.[5] The Raman spectrum of the ν_1 band, and its hot bands, of CCl_4 under static conditions is shown in Fig. 16a; the spectrum of CCl_4 in supersonic

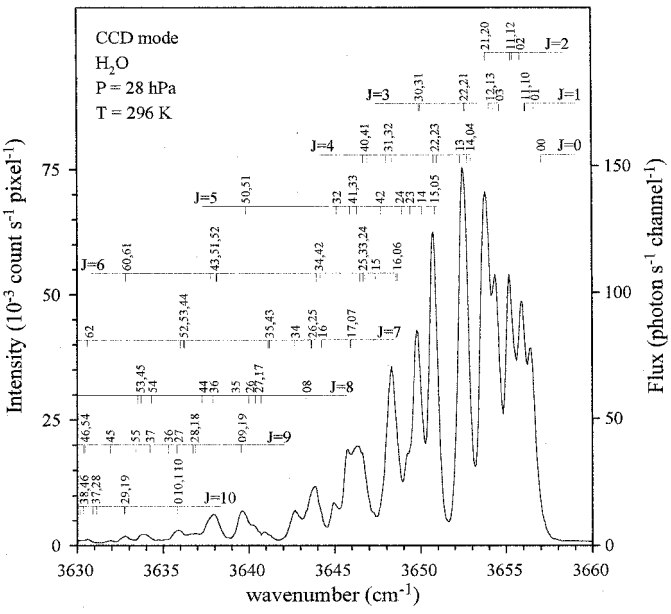

FIG. 15. Q-branch of the ν_1 Raman band of H_2O at 23 °C and P = 28 hPa, recorded in the CCD mode; laser power 2 W at 488.0 nm (+ multipass); slits: w_1 = 30 μm, h_1 = 10 mm, w_2 = 2600 μm; binning: n_h = 1 pixel, n_v = 180 pixels; average of 18 spectra at a rate of 1 min/spectrum. All lines are $\Delta J = 0$, $\Delta K_a = 0$, $\Delta K_c = 0$ transitions, labeled as K_aK_c for each value of J. Assignment based on the energy levels from Ref. 13. For overlapping transitions within each value of J, pairs of K_aK_c labels are arranged according to increasing wavenumbers.

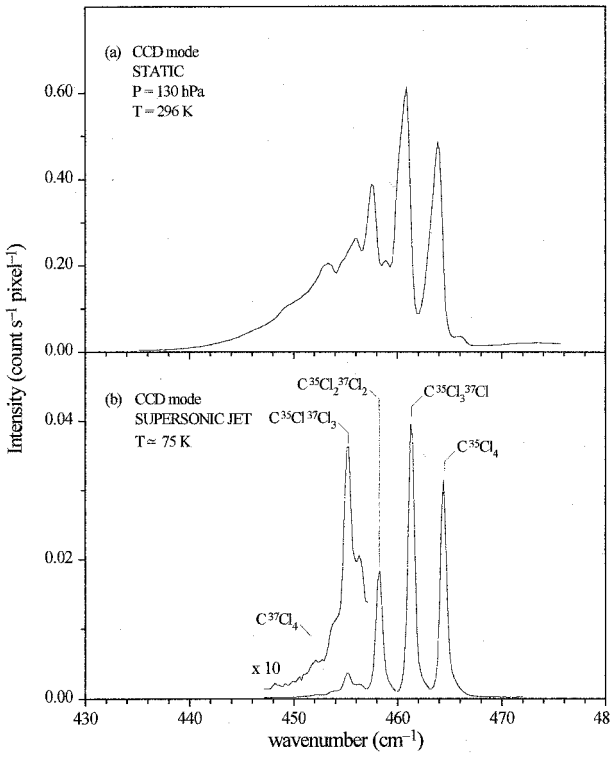

FIG. 16. Raman spectrum of the ν_1 band of CCl_4 in the gas phase recorded in the CCD mode. Laser power: 1.5 W at 514.5 nm (+ multipass + notch filter); slits: w_1 = 50 μm, h_1 = 20 mm, w_2 = 2600 μm; binning: n_h = 2 pixels, n_v = 200 pixels. **(a)** Static sample at its vapor pressure P = 130 hPa at T = 23 °C, average of N = 6 spectra at a rate of 2 min/spectrum; **(b)** in supersonic jet expansion through a Φ = 300 μm circular nozzle using N_2 as carrier gas; average of N = 10 spectra at a rate of 1 min/spectrum.

expansion, with N_2 as a carrier gas, is shown in Fig. 16b. The temperature estimated for this spectrum is $T \simeq 75$ K, with a molecular density number of CCl_4 of about 10^{-2} with respect to that of the equilibrium vapour pressure at 23 °C. In a comparison with the room-temperature spectrum in Fig. 16a, it can be seen how the strong and broad contribution from the $(\nu_1 + n\nu_4) - n\nu_4$, $(\nu_1 + n\nu_3) - n\nu_3$, and $(\nu_1 + n\nu_2) - n\nu_2$ hot bands almost completely disappears in the spectrum recorded under supersonic expansion.

In the spectra recorded under a resolution of ~ 0.5 cm^{-1} or better, a systematic distortion of the band shapes has been observed, consisting of an asymmetric broadening of the bands towards the red. The effect can clearly be observed in the spectra of Figs. 8, 9, 10, 14, and 16b. This undesired distortion appears not to be related to optical aberrations of the spectrometer, but to a lack of optimization of the charge transfer between neighbor pixels along the readout process, and is particularly noticeable for signals covering a reduced number of columns of pixels,[16] as is the case at a resolution of better than 0.5 cm^{-1}, where the FWHM of the signal corresponds to 4 pixels or less. This effect can in part be corrected by appropriate optimization of the internal CCD voltage settings, which are a function of the working temperature. Such an optimization has not been attempted in the scope of present work.

CONCLUSION

The spectra in Figs. 6–16, recorded with the instrument described in the second section of this paper, are meant to provide a useful reference for current and future developments in Raman instrumentation. We have shown to what extent the sensitivity of Raman spectroscopy can be improved on the basis of the currently available CCD detection technology, new optical and mechanical designs, and software developments. A gain of almost two orders of magnitude is attained, compatible with a scanning accuracy of better than ± 0.1 cm^{-1} and a spectral resolution of better than 0.3 cm^{-1} over a spectral range of more than 7000 cm^{-1}. In addition to this benefit, the original performance of the instrument as a single-channel subtractive double monochromator is entirely preserved, confering a great flexibility to the instrument at no extra cost. Spectrometers based on the principles shown here can widen considerably the scope of Raman spectroscopy to practical applications where a high sensitivity and a broad spectral range are mandatory. In terms of molecular species concentration, a detection threshold of about 1 ppm with respect to 100 kPa of gas sample is shown to be an affordable goal for present day Raman spectroscopy. Its equivalent, in terms of Raman photon flux, is in the range of 0.1 photon s^{-1} channel^{-1}. Such thresholds open interesting possibilities for gas-phase diagnosis, and for very low temperature spectroscopy in the gas phase,[5] widening the scope of Raman spectroscopy beyond traditional analytical applications or studies in the field of the molecular structure and dynamics.

ACKNOWLEDGMENTS

Thanks are due to D. Bermejo and R. Escribano for helpful comments and revision of the manuscript. The Dirección General de Investigación Científica y Técnica (DGICYT), of Spain, is acknowledged for financial support (Research Project PB91-0133).

1. V. Deckert and W. Kiefer, Appl. Spectrosc. **46,** 322 (1992).
2. K. C. Lepla and G. Horlick, Appl. Spectrosc. **44,** 1259 (1990).
3. W. Kiefer, H. J. Bernstein, H. Wieser, and M. Danyluk, J. Molec. Spectrosc. **43,** 393 (1972).
4. G. Tejeda, B. Maté, J. M. Fernández-Sánchez, and S. Montero, Phys. Rev. Lett. **76,** 34 (1996).
5. G. R. Phillips and J. M. Harris, Anal. Chem. **62,** 2351 (1990).
6. L. Kay and D. A. Sadler, Meas. Sci. Technol. **2,** 532 (1991).
7. W. Hill and D. Rogalla, Anal. Chem. **64,** 2575 (1992).
8. L. Kay, Meas. Sci. Technol. **3,** 400 (1992).
9. N. Papineau and M. Pealat, J. Chem. Phys. **79,** 5758 (1983).
10. K. Srinivasan, H. Finsterhölzl, H. W. Klöckner, D. Illig, and H. W. Schrötter, Z. Naturforsch. **32a,** 1070 (1977).
11. H. Finsterhölzl, H. W. Klöckner, K. Srinivasan, H. W. Schrötter, and J. Brandmüller, Indian J. Pure Appl. Phys. **16,** 370 (1978).
12. W. F. Murphy, Molec. Phys. **36,** 727 (1978).
13. J. M. Flaud and C. Camy-Peyret, Molec. Phys. **26,** 811 (1973); J. Molec. Spectrosc. **51,** 142 (1974).
14. I. F. Silvera and F. Tommasini, Phys. Rev. Lett. **37,** 136 (1976).
15. G. Luijks, S. Stolte, and J. Reuss, Chem. Phys. **62,** 217 (1981).
16. G. Béal, G. Boucharlat, J. Chabbal, J. P. Dupin, B. Fort, and Y. Mellier, Opt. Engin. **26,** 902 (1987).